metals

Article

Thermal Stability of the Precipitates in Dilute Al-Er-Zr/Hf Alloys at Elevated Temperature

Hao Wu [1],*, Qi Zhang [1],*, Li Li [1], Mingdong Huang [1],*, Zhikai Zheng [1] and Shengping Wen [2]

1   Chinalco Materials Application Research Institute Co., Ltd., Beijing 102209, China; lili@cmari.com (L.L.); zhengzhikai@cmari.com (Z.Z.)
2   School of Materials Science and Engineering, Beijing University of Technology, Beijing 100124, China; wensp@bjut.edu.cn
*   Correspondence: wuhao2469@126.com (H.W.); zhangqi@cmari.com (Q.Z.); huangmingdong@cmari.com (M.H.)

Abstract: The temporal evolution of microhardness and $Al_3(Er,Zr/Hf)$ precipitates are investigated in Al-Er-Zr/Hf alloys during annealing at 450 °C and 500 °C. The microhardness of the alloys decreases continuously with the prolonged annealing time due to the coarsening of the precipitates. Different weakening amplitudes are observed because of the disparity of the precipitate coarsening rate that is related to the disparity in their intrinsic diffusivities of Er, Zr, and Hf solute atoms in an Al matrix. The addition of Hf element is beneficial to enhancing the coarsening resistance, thus improving the thermal stability of the alloys. Introducing such elements to improve the thermal stability of precipitates can provide a new idea or choice for the development of heat-resistant aluminum alloys.

Keywords: Al-Er-Zr/Hf alloys; microhardness; precipitate; thermal stability; diffusion

1. Introduction

Aluminum alloys are widely applied in many industrial fields that require light-weight structural materials with adequate strength. However, their strength sharply deteriorates at elevated temperatures, which limits their application. For instance, the tensile strength of 7075 alloy at 200 °C and 300 °C is only about 30% and 10% of that at room temperature [1]. Intensive research has found that the rapid decline in mechanical properties is mainly due to a coarsening of the precipitates contributing to the alloy strength [2,3]. Therefore, the thermal stability of the strengthening precipitates in alloys at an elevated temperature is the key factor in the design and development of heat-resistant aluminum alloys.

Introducing coherent precipitates such as the $L1_2$-structured intermetallics in aluminum alloys through microalloying can effectively improve the thermal stability of alloys. In Al-Sc alloys, the Al_3Sc precipitates are extremely stable at 300 °C and will not grow significantly even after hundreds of hours of thermal exposure [2]. Adding trace Ti, Zr, Hf, or other elements with slower diffusion rates in Al-Sc alloys can form nanoscale spheroidal $L1_2$-structured $Al_3(Sc,M)$ precipitates [4–14]. These precipitates have a complex core–shell structure, which possesses excellent thermal stability. In addition, it is reported that the additions of Y, Sm, Hf, Er, and Gd enhance the thermal stability of the $Al_3(Sc,Zr)$ dispersoids, maintain the hardness or tensile properties after annealing at 250~370 °C with a hold of up to 100 h, and can eliminate the negative effects of Fe and silicon impurities [13–15].

The precipitation strengthening in dilute Al-Er-Zr, Al-Er-Hf, and Al-Er-Zr-Hf alloys has been investigated in our previous research work [15–17]. In this article, the temporal evolution of microhardness and the $Al_3(Er,Zr/Hf)$ precipitates' characteristics in Al-Er-Zr/Hf alloys are investigated during annealing at 450 °C and 500 °C in order to provide a new idea for the design of heat-resistant aluminum alloys.

2. Material and Methods

The composition of Al-0.04Er-0.08Zr, Al-0.04Er-0.18Hf, and Al-0.04Er-0.08Zr-0.1Hf (at. %) alloys was prepared by ingot metallurgy; the size of the ingot was about $30 \times 90 \times 150$ mm^3. The castings were homogenized at 640 °C for 24 h and water-quenched, followed by isothermal annealing at 350 °C to a peak hardness state. After that, the peak hardness samples were annealed at 450 °C for 100 h and subsequently annealed at 500 °C for 100 h. The samples were water-quenched after each heating step. The precipitation hardening effect during elevated temperature annealing was monitored by Vickers microhardness.

Vickers microhardness measurements were carried out on polished samples using a HXD-1000TM/LCD hardness tester with a load of 200 g and a dwell time of 10 s. The microstructural evolution of as-homogenized samples was characterized using FEI Quanta 650 FEG scanning electron microscope (SEM), and the precipitation evolution was investigated using a JEOL 2100 with an operating voltage of 200 kV. The size (diameter) of precipitates under each condition was analyzed using Image-Pro Plus software.

3. Results and Discussion

3.1. Microhardness Evolution during Annealing

The Vickers microhardness evolution of Al-0.04Er-0.08Zr, Al-0.04Er-0.18Hf, and Al-0.04Er-0.1Hf-0.08Zr alloys during isothermal annealing at 350 °C is shown in Figure 1a, which is from our previous research work [15–17]. In this experiment, the initial hardness of peak hardness samples was 57.6 ± 0.7 HV, 66.0 ± 1.3 HV, and 65.9 ± 1.4 HV for Al-Er-Zr, Al-Er-Hf, and Al-Er-Zr-Hf alloy, respectively. The microhardness evolution of the peak hardness samples during annealing at 450 °C is displayed in Figure 1b. It can be seen that, with the extension of annealing time, the microhardness of the alloys decreases continuously, but the decreasing amplitudes are different. After annealing at 450 °C for 100 h, the microhardness decreases by about 18.2 HV from 57.6 ± 0.7 HV to 39.4 ± 0.8 HV for the Al-Er-Zr alloy and by about 18.4 HV from 66.0 ± 1.4 HV to 47.6 ± 1.0 HV for the Al-Er-Zr-Hf alloy, respectively. The Al-Er-Hf alloy exhibits better thermal stability with only about a 12.9 HV decline in microhardness, from 66.0 ± 1.3 HV to 53.0 ± 1.0 HV.

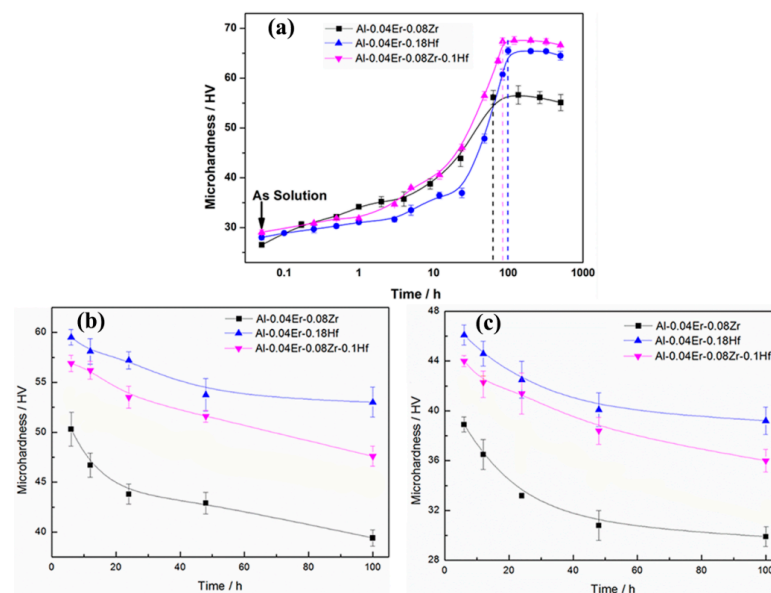**Figure 1.** Microhardness evolution vs. exposure time: (**a**) at 350 °C (Reprinted/adapted with permission from Ref. [17]. 2015, Elsevier. ©); (**b**) at 450 °C after annealing at 350 °C to the peak hardness state, and (**c**) at 500 °C after annealing at 450 °C for 100 h.

Under further annealing at 500 °C, the microhardness of the samples decreases significantly during the first 50 h and becomes stables after that, as shown in Figure 1c. The microhardness of the Al-Er-Zr alloy annealed for 100 h decreases to 29.9 ± 0.8 HV, which is close to the microhardness of the as-homogenized state [15]. However, the microhardness of the Hf-containing alloys, Al-Er-Zr-Hf and Al-Er-Hf, remains 36.0 ± 0.9 HV and 40.2 ± 1.4 HV, respectively, which is significantly higher than that of the Al-Er-Zr alloy. This indicates that the addition of Hf element is beneficial for enhancing the thermal stability of the alloys.

3.2. Microstructural Evolution during Annealing

The as-homogenized and peak hardness state of the Al-Er-Hf alloy was selected for microstructure analysis due to the relatively high composition. Some residual lamellar eutectic structures were located on the grain boundaries in the as-homogenized alloy, as shown in Figure 2a. A round-shaped eutectic structure (AlErHf ternary), whose size was approximately 1 µm, can be seen in Figure 2c. A high number density of homogeneously distributed, nearly spherical precipitates can be seen in Figure 2d, which are the micrographs of the Al-Er-Hf alloy isothermally annealed to peak hardness.
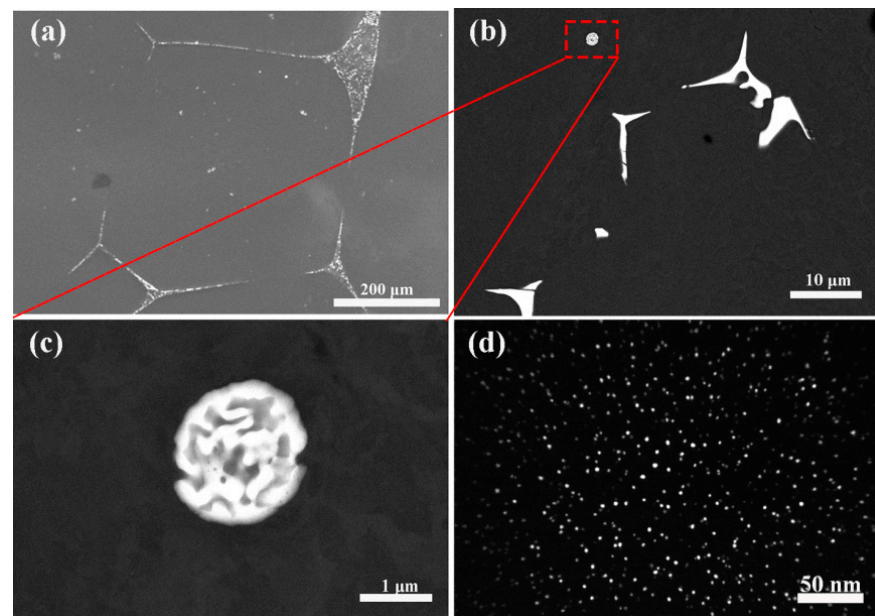

Figure 2. Micrographs of Al-Er-Hf alloy: (**a**–**c**) SEM micrographs of as-homogenized alloy; (**d**) dark-field TEM micrographs of precipitates of the peak aging alloy.

Generally, the strengthening effect of the alloy is related to the precipitates' characteristics, such as size and volume fraction. In order to explore the difference between the precipitates in the three alloys, the TEM micrographs of precipitates, i.e., the Al_3(Er,Zr), Al_3(Er,Hf), and Al_3(Er,Zr,Hf) particles, which are identified by energy dispersive X-ray spectrometry (EDX), are presented in Figure 3. It can be found that all precipitates were spherical under the different annealing conditions. According to the selected area electron diffraction (SAED) pattern of precipitates (Figure 3c), it can be concluded that these precipitates have an $L1_2$ crystal structure. However, the number density of precipitates obviously decreases with the coarsening of the precipitate after 500 °C annealing, especially in the Al-Er-Zr alloy.
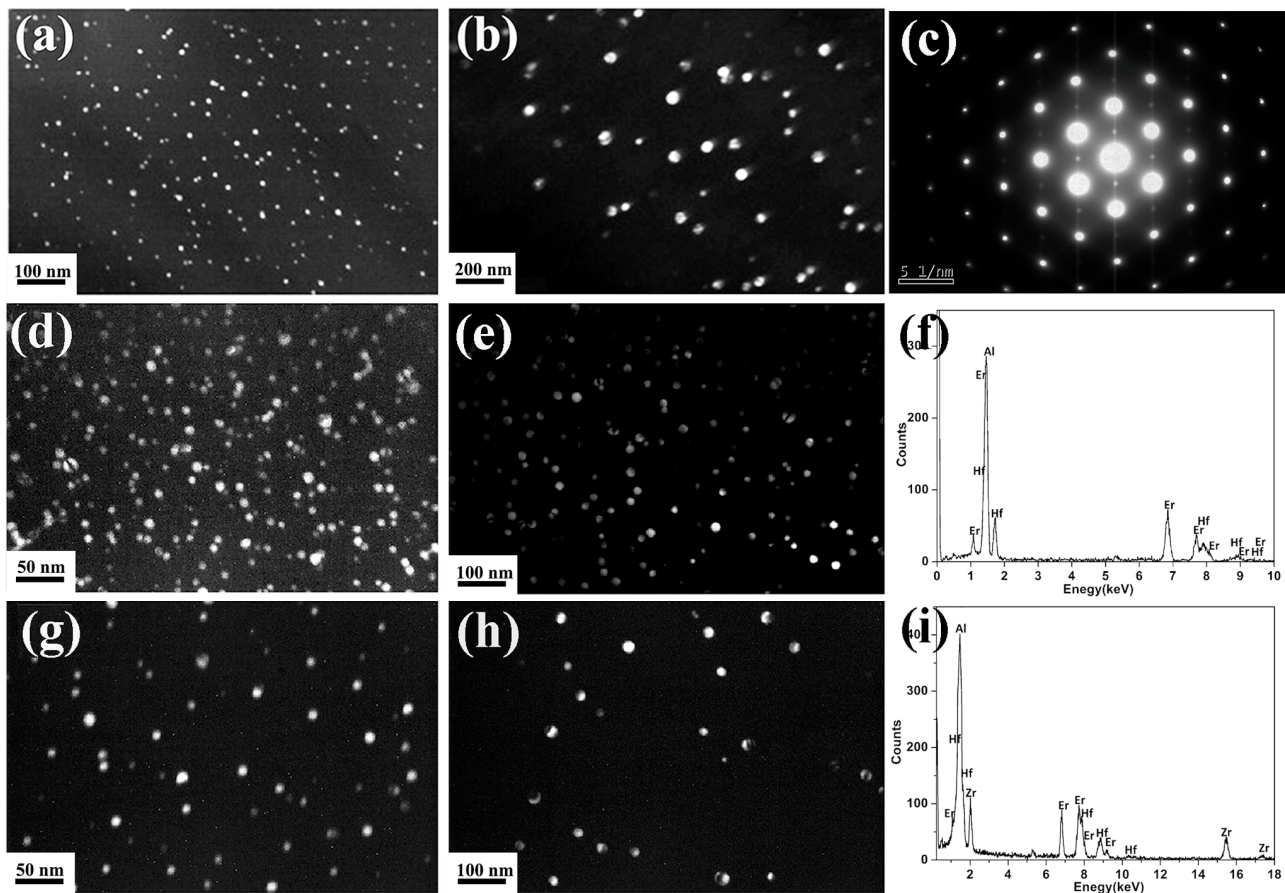
Figure 3. Dark-field TEM micrographs of precipitates: (**a,d,g**) Al-Er-Zr, Al-Er-Hf, and Al-Er-Zr-Hf alloy annealed at 450 °C for 100 h; (**b,e,h**) Al-Er-Zr, Al-Er-Hf, and Al-Er-Zr-Hf alloy annealed at 500 °C for 100 h after being annealed at 450 °C for 100 h; (**c**) the SAED pattern of precipitates; (**f,i**) EDX analysis of precipitates.

The detailed precipitate size and number density for the three alloys during different annealing stages are listed in Table 1. For all alloys, the precipitate size gradually increases with the annealing time for a given temperature. As listed in the table, although the precipitate diameters for the Al-Er-Zr, Al-Er-Hf, and Al-Er-Zr-Hf alloys at a peak hardness state are similar (about 3.6 ± 0.1 nm, 3.9 ± 0.2 nm, and 3.4 ± 0.1 nm, respectively), the coarsening rate of $Al_3(Er,Zr)$ particles in the Al-Er-Zr alloy is faster than that of $Al_3(Er,Hf)$ and $Al_3(Er,Zr,Hf)$ particles in the Hf-containing alloys. The average diameter of precipitates in Al-Er-Zr, Al-Er-Hf, and Al-Er-Zr-Hf alloys increases to 11.2 ± 1.6 nm, 8.1 ± 0.2 nm, and 8.7 ± 0.2 nm after annealing at 450 °C for 100 h, and grows further to 42.9 ± 2.6 nm, 19.4 ± 0.3 nm, and 20.8 ± 1.1 nm after annealing at 500 °C for 100 h, respectively. Hardness is directly related to volume fraction and particle size. In our case, the Orowan bypass mechanism should be responsible for the particle-induced strengthening, the strength is directly proportional to volume fraction and inversely proportional to particle size, and the volume fraction is proportional to the number density of particles. With the increase in annealing temperature and time, the number density of precipitates decreases and the particle size increases; therefore, the coarsening of the precipitates will weaken the strengthening effect of alloys and directly result in the continuous dropping of the corresponding microhardness.

Table 1. The average diameter and number density of precipitates after various annealing.

Temperature and Time (°C and h)		Al-Er-Zr		Al-Er-Hf		Al-Er-Zr-Hf	
		d/nm	Nv/10^{21}	d/nm	Nv/10^{21}	d/nm	Nv/10^{21}
Peak hardness state		3.6 ± 0.1	27 ± 5.1	3.9 ± 0.2	32.9 ± 6.7	3.4 ± 0.1	43.0 ± 8.8
450	5	4.5 ± 0.8	23 ± 3.2	—		—	
	6	—		4.3 ± 0.1	18.9 ± 1.6	3.6 ± 0.1	24.6 ± 5.0
	12	6.1 ± 0.8	18 ± 2.6	—		—	
	48	9.6 ± 1.4	8.1 ± 1.9	6.5 ± 0.1	12.7 ± 1.8	6.5 ± 0.2	10.2 ± 2.1
	100	11.2 ± 1.6	3.2 ± 0.8	8.1 ± 0.2	11.5 ± 2.3	8.7 ± 0.2	5.0 ± 2.1
500	5	19.5 ± 1.3	1.9 ± 0.2	—		—	
	6	—		8.5 ± 0.1	5.1 ± 1.0	9.1 ± 0.2	4.7 ± 0.9
	12	24.9 ± 1.6	0.7 ± 0.1	8.7 ± 0.2	4.7 ± 0.9	10.0 ± 0.2	3.8 ± 0.8
	24	—		12.7 ± 0.3	3.7 ± 0.8	13.2 ± 0.3	3.0 ± 0.6
	48	31.5 ± 2.0	0.2 ± 0.1	15.2 ± 0.3	3.5 ± 0.7	17.4 ± 0.3	0.6 ± 0.1
	100	42.9 ± 2.6	0.1 ± 0.1	19.4 ± 0.3	2.4 ± 0.5	20.8 ± 1.1	0.6 ± 0.1

3.3. Coarsening Resistance of Precipitates

Lifshitz, Slyozov, and Wagner proposed a classic coarsening model controlled by volume diffusion (LSW model) that can predict the coarsening kinetics of the alloys. According to the LSW coarsening model, the average particle size d(t) and coarsening time t should conform to the following relationship [18,19]:

$$d(t) - d(t_0) = K\left(t^{1/3} - t_0^{1/3}\right) \tag{1}$$

where K is the coarsening rate, $d(t_0)$ is the average particle size at t_0, and t_0 is any time at or after the initiation of quasi-stationary state coarsening.

The mean precipitate diameter changes versus the cube-root of the time at a given temperature can be well linear fitted, as plotted in Figure 4, which indicates that the precipitates in all alloys have similar coarsening kinetics. The slope of the fitted line can be considered as the coarsening rate of the precipitates. As anticipated, the coarsening rate of precipitates is faster at a higher temperature for each alloy. For example, the coarsening rate of Al$_3$(Er,Zr) particles in the Al-Er-Zr alloy isothermally annealed at 500 °C is 7.26 ± 0.99 nm/h$^{1/3}$, compared with a much lower value of only 2.40 ± 0.16 nm/h$^{1/3}$ at 450 °C. This is mainly due to the increase in the solute diffusion rate with a temperature rise, leading to faster precipitate growth and coarsening rate. Furthermore, the addition of Hf element will further enhance the coarsening resistance of precipitates and improve the thermal stability of the Hf-containing alloys. The Al$_3$(Er,Hf) particles in the Al-Er-Hf alloy show a much more outstanding thermal stability than the Al$_3$(Er,Zr,Hf) particles in the Al-Er-Zr-Hf alloy and the Al$_3$(Er,Zr) particles in the Al-Er-Zr alloy. Compared with the Al-Er-Zr alloy, the slope of the fitted line gradually reduces with the increase in Hf element content. It can be seen from the plot that the coarsening rate of precipitates in the Al-Er-Zr-Hf and Al-Er-Hf alloys annealed at 500 °C is about 4.71 ± 0.55 nm/h$^{1/3}$ and 3.95 ± 0.29 nm/h$^{1/3}$, respectively.
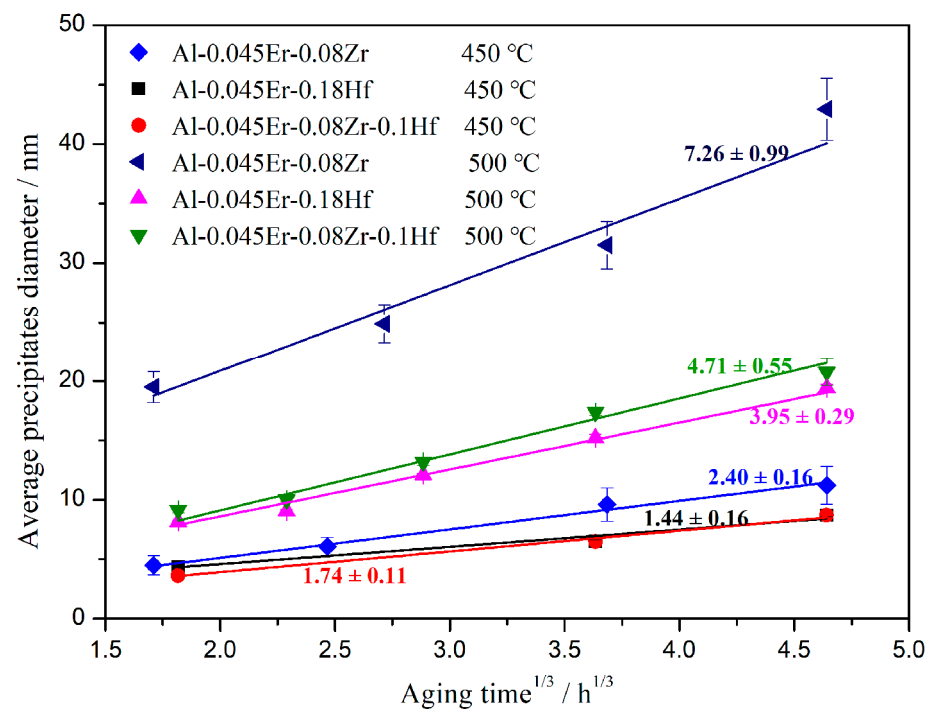
Figure 4. Average diameter of precipitates as a function of the cube root of the annealing time.

Intensive research demonstrates that such precipitates have a typical spherical core/shell structure and the nucleation and growth of precipitates are controlled by the synergy effects between joint added elements such as $Al_3(Sc,Zr)$ particles in the Al-Sc-Zr alloy [2,6,20] and $Al_3(Er,Sc,Zr)$ particles in the Al-Sc-Er-Zr alloy [21,22], etc. The difference in precipitate coarsening rates for each alloy studied in this work is mainly due to the diffusion-limited coarsening mechanism. The precipitate coarsening kinetics are closely related to the diffusivity of solute atoms in the Al matrix, and the diffusivity coefficient of solute in the Al matrix decreases from Er to Zr and Hf (i.e., $D_{Er} > D_{Zr} > D_{Hf}$) at 450 °C and 500 °C [16]. The Zr or Hf element will segregate to the already-nucleated Er-enriched precipitate interfaces and form an enveloping Zr/Hf-enriched shell, which can be a barrier to the growth and coarsening of precipitates during prolonged thermal exposure, thus further delaying the deterioration of mechanical properties.

The diffusion distance of the solute atoms in the Al matrix can be simply calculated by a root-mean-square (RMS) diffusion distance, $\sqrt{4Dt}$ (D is the diffusion coefficient of solute at a given temperature and t is annealing time), as shown in Figure 5. The RMS diffusion distance of Er, Zr, and Hf solute atoms at a given temperature increases continuously with prolonged annealing time; the Er element is the most significant, followed by the Zr element, which is the main reason that the coarsening rate of nanoprecipitates in the Al-Er-Zr/Hf alloys exhibit significant differences, i.e., $Al_3(Er,Zr) > Al_3(Er,Zr,Hf) > Al_3(Er,Hf)$. Therefore, combined with the corresponding precipitate evolution, the distinct difference in microhardness weakening behaviors can be well explicated by the disparity of precipitate coarsening rates dominated by diffusivities of the solute elements in the Al matrix. The high thermal stability of the $Al_3(Er,Zr/Hf)$ precipitates in dilute Al-Er-Zr/Hf alloys at elevated temperatures can provide a new idea for the design of heat-resistant aluminum alloys.
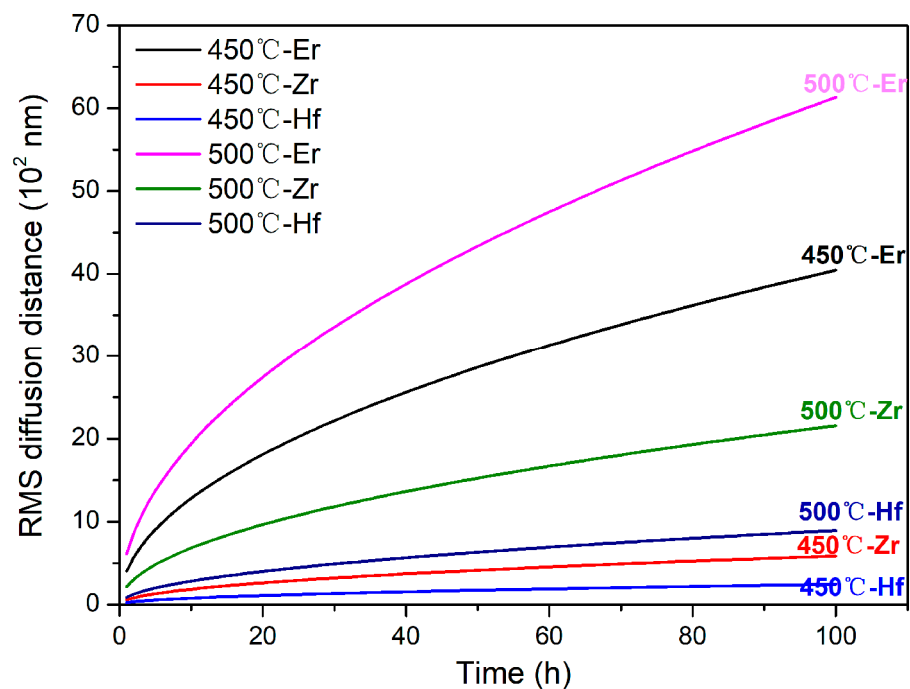
Figure 5. The RMS diffusion distance of Er, Zr, and Hf solute atoms in Al matrix at 450 °C and 500 °C.

4. Conclusions

In summary, the microhardness of each alloy continuously decreases with the extension of annealing time, but the decreasing amplitudes are different. The distinct difference in microhardness weakening behaviors of the alloys can be well explicated by the disparity of the precipitate coarsening rate. Due to the diffusivity coefficient of solute in the Al matrix decreasing from Er to Zr and Hf, the $Al_3(Er,Hf)$ particles in the Al-Er-Hf alloy have a much more outstanding coarsening resistance than the $Al_3(Er,Zr,Hf)$ and the $Al_3(Er,Zr)$ particles in the Al-Er-Zr-Hf and Al-Er-Zr alloys, respectively. The addition of the Hf element is beneficial for enhancing the thermal stability of the alloys. The Al-Er-Hf and Al-Er-Zr-Hf alloys exhibit more excellent thermal stability than that of the Al-Er-Zr alloy.

Author Contributions: H.W.: writing—original draft, writing—review and editing; Q.Z.: investigation; L.L.: methodology; M.H.: project administration; Z.Z.: methodology; S.W.: formal analysis. All authors have read and agreed to the published version of the manuscript.

Institutional Review Board Statement: Not applicable.

Informed Consent Statement: Not applicable.

Data Availability Statement: Not applicable.

Conflicts of Interest: The authors have no conflict of interest.

References

1. Polmear, I.J.; Couper, M.J. Design and development of an experimental wrought aluminum alloy for use at elevated temperatures. *Metall. Trans.* **1988**, *19*, 1027–1035. [CrossRef]
2. Fuller, C.B.; Seidman, D.N. Temporal evolution of the nanostructure of Al (Sc,Zr) alloys: Part II-coarsening of $Al_3(Sc_{1-x}Zr_x)$ precipitates. *Acta Mater.* **2005**, *53*, 5415–5428. [CrossRef]
3. Gao, Y.H.; Liu, G.; Sun, J. Recent progress in high-temperature resistant aluminum-based alloys: Microstructural design and precipitation strategy. *Acta Metall. Sin.* **2021**, *57*, 129–149.
4. van Dalen, M.E.; Dunand, D.C.; Seidman, D.N. Effects of Ti additions on the nanostructure and creep properties of precipitation-strengthened Al-Sc alloys. *Acta Mater.* **2005**, *53*, 4225–4235. [CrossRef]

5. van Dalen, M.E.; Dunand, D.C.; Seidman, D.N. Creep-and coarsening properties of Al-0.06 at.% Sc-0.06 at.% Ti at 300–450 °C. *Acta Mater.* **2008**, *56*, 4369–4377. [CrossRef]

6. Fuller, C.B.; Murray, J.L.; Seidman, D.N. Temporal evolution of the nanostructure of Al(Sc,Zr) alloys: Part I-Chemical compositions of $Al_3(Sc_{1-x}Zr_x)$ precipitates. *Acta Mater.* **2005**, *53*, 5401–5413. [CrossRef]

7. Hallem, H.; Lefebvre, W.; Forbord, B. The formation of $Al_3(Sc_xZryHf_{1-x-y})$-dispersoids in aluminium alloys. *Mater. Sci. Eng. A* **2006**, *421*, 154–160. [CrossRef]

8. Nokhrin, A.; Shadrina, I.; Chuvil'deev, V.; Kopylov, V.; Berendeev, N.; Murashov, A.; Bobrov, A.; Tabachkova, N.; Smirnova, E.; Faddeev, M. Investigation of thermal stability of microstructure and mechanical Properties of bimetallic fine-grained wires from Al-0.25%Zr-(Sc,Hf) alloys. *Materials* **2022**, *15*, 185. [CrossRef]

9. Barkov, R.Y.; Pozdniakov, A.V.; Tkachuk, E.; Zolotorevskiy, V.S. Effect of Y on microstructure and mechanical properties of Al-Mg-Mn-Zr-Sc alloy with low Sc content. *Mater. Lett.* **2018**, *217*, 135–138. [CrossRef]

10. Pozdniakov, A.V.; Yarasu, V.; Barkov, R.Y.; Yakovtseva, O.A.; Makhov, S.V.; Napalkov, V.I. Microstructure and mechanical properties of novel Al-Mg-Mn-Zr-Sc-Er alloy. *Mater. Lett.* **2017**, *202*, 116–119. [CrossRef]

11. Barkov, R.Y.; Mikhaylovskaya, A.V.; Yakovtseva, O.A.; Loginova, I.S.; Prosviryakov, A.S.; Pozdniakov, A.V. Effects of thermomechanical treatment on the microstructure, precipitation strengthening, internal friction, and thermal stability of Al-Er-Yb-Sc alloys with good electrical conductivity. *J. Alloys Compd.* **2021**, *855*, 157367. [CrossRef]

12. Pozdniakov, A.V.; Barkov, R.Y. Microstructure and mechanical properties of novel Al-Y-Sc alloys with high thermal stability and electrical conductivity. *J. Mater. Sci. Technol.* **2020**, *36*, 1–6. [CrossRef]

13. Pozdniakov, A.V.; Aytmagambetov, A.A.; Makhov, S.V.; Napalkov, V.I. Effect of impurities of Fe and Si on the structure and strengthening upon annealing of the Al-0.2%Zr-0.1%Sc alloys with and without Y additive. *Phys. Met. Metall.* **2017**, *118*, 479–484. [CrossRef]

14. APozdnyakov, V.; Osipenkova, A.A.; Popov, D.A.; Makhov, S.V.; Napalkov, V.I. Effect of Low Additions of Y, Sm, Gd, Hf and Er on the Structure and Hardness of Alloy Al-0.2%Zr-0.1%Sc. *Met. Sci. Heat Treat.* **2017**, *58*, 537–542. [CrossRef]

15. Wen, S.P.; Gao, K.Y.; Li, Y.; Huang, H.; Nie, Z.R. Synergetic effect of Er and Zr on the precipitation hardening of Al-Er-Zr alloy. *Scr. Mater.* **2011**, *65*, 592–595. [CrossRef]

16. Wu, H.; Wen, S.P.; Gao, K.Y.; Huang, H.; Wang, W.; Nie, Z.R. Effect of Er additions on the precipitation strengthening of Al-Hf alloys. *Scr. Mater.* **2014**, *87*, 5–8. [CrossRef]

17. Wu, H.; Wen, S.P.; Wu, X.L.; Gao, K.Y.; Huang, H.; Wang, W.; Nie, Z.R. A study of precipitation strengthening and recrystallization behavior in dilute Al-Er-Hf-Zr alloys. *Mater. Sci. Eng. A* **2015**, *639*, 307–313. [CrossRef]

18. Philippe, T.; Voorhees, P.W. Ostwald ripening in multicomponent alloy. *Acta Mater.* **2013**, *61*, 4237–4244. [CrossRef]

19. Pletcher, B.A.; Wang, K.G.; Glicksman, M.E. Experimental, computational and theoretical studies of δ' phase coarsening in Al-Li alloys. *Acta Mater.* **2012**, *60*, 5803–5817. [CrossRef]

20. Xue, N.; Liu, W.; Zhu, L.; Muthuramalingam, T. Effect of scandium in Al-Sc and Al-Sc-Zr alloys under precipitation strengthening mechanism at 350 °C Aging. *Met. Mater. Int.* **2021**, *27*, 5145–5153.

21. Booth-Morrison, C.; Dunand, D.C.; Seidman, D.N. Coarsening resistance at 400 °C of precipitation-strengthened Al-Zr-Sc-Er alloys. *Acta Mater.* **2011**, *59*, 7029–7042. [CrossRef]

22. Liu, L.; Jiang, J.T.; Cui, X.Y.; Zhang, B.; Zhen, L.; Ringer, S.P. Correlation between precipitates evolution and mechanical properties of Al-Sc-Zr alloy with Er additions. *J. Mater. Sci. Technol.* **2022**, *99*, 61–72. [CrossRef]